

Supplementary Materials

Performing Calculus: Asymmetric Adaptive

Stimuli-Responsive Material for Derivative Control

Spandhana Gonuguntla,^{1†} Wei Chun Lim,^{1†} Fong Yew Leong,² Chi Kit Ao,¹

Changhui Liu,¹ and Siowling Soh^{1*}

¹ Department of Chemical and Biomolecular Engineering, National University of

Singapore, 4 Engineering Drive 4, Singapore 117585, Singapore

² A*STAR Institute of High Performance Computing, 1 Fusionopolis Way, Connexis,

138632, Singapore

[†] These authors contributed to this work equally.

* To whom correspondence may be addressed: chessl@nus.edu.sg

Short Title: Derivative Control by Stimuli-Responsive Material

1. Characterization of materials

Optimizing the thickness of material. We tested the different thicknesses of the layers of hydrogel and elastomer for fabricating the asymmetric stimuli-responsive material. In general, the layer of elastomer needed to be sufficiently thin so that the asymmetric stimuli-responsive material could have the unique material property of being highly adaptive. The hydrogel also needed to be thin so that the material responded quickly. After investigating the different thicknesses, we eventually chose the relatively thin thickness of the hydrogel to be 160 μm and extremely thin layer (i.e., thickness of $<1 \mu\text{m}$) of elastomer obtained by spin-coating the layer of elastomer over the hydrogel at 5000 rpm. For the investigation of the thickness of the composite material, we tested the case when the thickness of the elastomer was large when a low spin speed was used during the process of spin-coating the elastomer onto the hydrogel. A low spin speed gave rise to a thicker layer of elastomer. With lower spin speeds (e.g., 1000 rpm and 3000 rpm), the material was a bilayer: when the hydrogel expanded in a pH 12 solution, the material remained in the bent state at steady state. Hence, the large thickness caused the elastomer to have significant mechanical influence over the bending of the material. When the hydrogel was thick (e.g., 400 μm for the same thickness of the elastomer of $<1 \mu\text{m}$), the time of response of the asymmetric stimuli-responsive material was much longer. Specifically, for the experiment that involved changing the pH from deionized water to pH 12 rapidly, it took around 2.5 days to undergo a complete transition from being initially flat, to a bent state, and back to being flat again, compared to the few hours that we reported in the main text (i.e., Fig. 2B). These results are summarized in Table S2.

Previous works have reported bilayers that consist of a layer of stimuli-responsive hydrogel and a layer of non-responsive elastomer (43, 44). However, the thickness of the layer of elastomer reported in these previous studies is always comparable to the thickness

54 of the stimuli-responsive hydrogel; hence, the bending of these bilayers depends on the
55 magnitude of the stimulus. In other words, the bilayers are not adaptive like our
56 asymmetric stimuli-responsive material. Our method of coating the elastomer over the
57 stimuli-responsive hydrogel is simple and general. Specifically, the elastomer can be
58 coated over the surface of any type of hydrogel and the thickness of the elastomer can be
59 easily tunable via the spin-coating process using our method.

60
61 **Analysis of the Chemical Compositions of the Materials.** We analyzed the chemical
62 compositions of the dried pH-responsive hydrogel, glucose-responsive hydrogel, and the
63 elastomer by FTIR. The FTIR spectrum was recorded by a Vertex 70 spectrometer
64 (Bruker, USA) using the Attenuated Total Reflectance (ATR) mode. The analysis of the
65 pH-responsive hydrogel, p(DMAEMA-*co*-HEMA), showed the characteristic stretching
66 peak of the carbonyl group at 1707 cm⁻¹, tertiary amine at 1274 and 1248 cm⁻¹,
67 asymmetric C-H stretching peak at 2944 cm⁻¹, primary hydroxyl group at 3373 cm⁻¹,
68 alkoxy group represented by the C-O stretching peak at 1154 and 1024 cm⁻¹, and C-O-C
69 stretching peak at 1075 cm⁻¹ (fig. S3 and table S1) (45). Glucose-responsive hydrogel was
70 fabricated without entrapping the enzyme (i.e., glucose oxidase) for analyzing its
71 composition using FTIR. The p(MAA-*co*-HEMA) hydrogel showed its characteristic OH
72 stretching peak at 3384 cm⁻¹, C=O stretching peak at 1714 cm⁻¹, C-H stretching peak at
73 2884 cm⁻¹, alkoxy functional group showing the C-O stretching peak at 1022 and 1048
74 cm⁻¹, and C-O-C peak at 1075 cm⁻¹ (46). The Ecoflex™ elastomer showed its
75 characteristic (CH₃)₂-Si peak at 784 cm⁻¹, Si-O-Si stretching peak at 1006 and 1070 cm⁻¹,
76 Si-CH₃ stretching peak at 1257 cm⁻¹, and C-H stretching peak at 2962 cm⁻¹ (47).

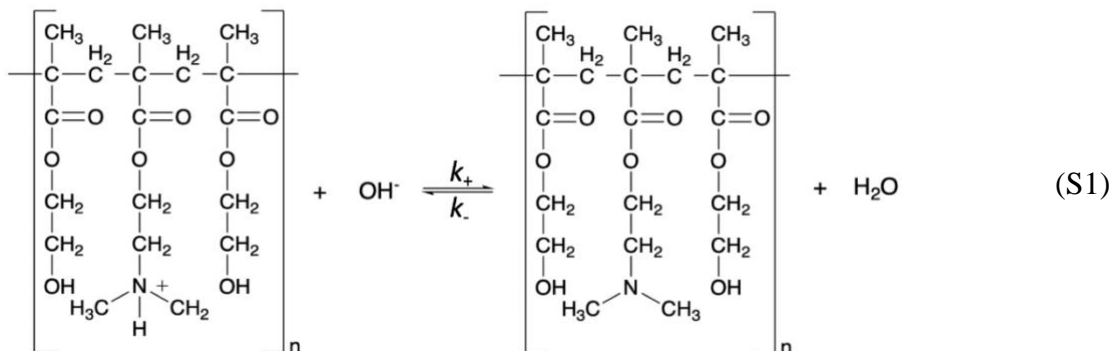
77

Mechanical characterization of the hydrogels. The elastic moduli of poly(DMAEMA-*co*-HEMA) hydrogel and poly(MAA-*co*-HEMA) were determined. The materials were subjected to a tensile test using the INSTRON 5542 (INSTRON, USA) tensile testing equipment operated at 2.5 mm/min displacement rate. The measurement data were collected using a 50 N load cell. The expanded hydrogels of poly(DMAEMA-*co*-HEMA) were tested to have an elastic modulus of 800 kPa, whereas the poly(MAA-*co*-HEMA) had an elastic modulus of 2050 kPa.

2. Modeling the Bending of the Asymmetric Stimuli-Responsive Hydrogel

The bending of the asymmetric pH-responsive hydrogel involves the diffusion of the OH⁻ ions into the hydrogel, reaction of the OH⁻ ions with the amine functional groups within the hydrogel, and the asymmetric contraction of the hydrogel. The equations for evaluating the unsteady-state reaction-diffusion process and curvature of the hydrogel due to the asymmetric contractile strain are stated as Equations (1) – (3) in the main text. This section provides more details of the parameters and method of solution used for the model.

Reaction of the OH⁻ ions and amine groups. The reaction between the OH⁻ ions from the medium and the amine functional groups within the hydrogel is shown in Equation (S1).



97 k_+ and k_- are the forward and backward rate constants of the reaction respectively. Acid-
98 base reactions are known to be extremely fast; hence, the process is diffusion limited. In
99 this case, only the ratio of the rate constants k_+/k_- is required in the model. Based on the
100 reported $pK_a = 7.25$ (48), we calculated $k_+/k_- = 10^{6.75}$.

101
102 **Initial concentration of amine groups.** The initial concentration of the protonated amine
103 groups in the pH-responsive hydrogel that is expanded in deionized water, s_0 , before any
104 reaction with the OH^- ions (i.e., when the pH of the medium is increased) is calculated as
105 follows. First, the mass of the pH-responsive hydrogel (1.5×2.5 mm and a thickness of 80
106 μm) immediately after polymerization was measured to be 0.34 mg. Because DMAEMA
107 made up 19.53 mol% (or an equivalent of 22.2 wt%) of the hydrogel, the mass of the
108 DMAEMA in the hydrogel was 76.3 μg , or an equivalent of 0.49 μmol . After immersing
109 the pH-responsive hydrogel in deionized water, the hydrogel expanded to a volume of
110 $V_{\text{expand}} = 2.4$ μL (with dimensions of 3×5 mm and a thickness of 160 μm). In its expanded
111 state, the amine groups in the hydrogel were expected to be mostly protonated. The
112 amount of amine groups protonated according to the equilibrium reaction (S1) can be
113 determined by the Henderson-Hasselbalch Equation (S2), where $[A]$ and $[A^+]$ represent the
114 concentration of the unprotonated and protonated amine groups respectively.

$$115 \quad pH = pK_a + \log \frac{[A]}{[A^+]} \quad (S2)$$

116 The Henderson-Hasselbalch Equation can be expressed in terms of the number of moles of
117 the unprotonated amine groups, n_A , and the number of moles of the protonated amine
118 groups, n_{A^+} , instead of the concentrations, according to Equation (S3).

$$119 \quad pH = pK_a + \log \frac{n_A/V}{n_{A^+}/V} = pK_a + \log \frac{n_A}{n_{A^+}} \quad (S3)$$

In this case, $\text{pH} \approx 6$ and $\text{pKa} = 7.25$ as discussed. Because we calculated that the total number of moles of the amine groups is $n_{\text{total}} = 0.49 \mu\text{mol}$, we can express the relationship between n_{A} and n_{A^+} according to Equation S4.

$$n_{\text{total}} = n_{\text{A}} + n_{\text{A}^+} = 0.49 \mu\text{mol} \quad (\text{S4})$$

By solving the two Equations S3 and S4, we found that $n_{\text{A}^+} = 0.46 \mu\text{mol}$. Because $s_0 = n_{\text{A}^+}/V_{\text{expand}}$, s_0 is calculated to be 0.19 M.

Logistic model for contractile strain. We have determined the sizes of the pH-responsive hydrogel at different pH at equilibrium (Fig. 3b in the main text). The contraction ratio was defined as L/L_{expanded} , where L is the length of the hydrogel after immersing it in a solution of a specific pH. L_{expanded} is the length of the expanded hydrogel in pH 2. The contractile strain, ε , was defined as $(L_{\text{expanded}} - L)/L_{\text{expanded}}$. The experimental data in Fig. 3b were replotted as the contractile strain against pH as shown in fig. S4. We fitted this set of experimental data with a logistic function that is expressed as $\varepsilon(\text{pH}) = \varepsilon_{\text{max}} \left[1 + 10^{-(\text{pH} - \text{pH}_{\text{mid}})} \right]^{-1}$, where pH_{mid} is the pH at mid-strain and ε_{max} is the maximum strain. From the best fit curve, we obtained $\text{pH}_{\text{mid}} = 9.4$ and $\varepsilon_{\text{max}} = 2.8$ (fig. S7). On the other hand, the model used concentration as the variable, not pH. Therefore, for the purpose of modelling the bending of hydrogel, the logistic function that relates contractile strain to pH is converted to the relationship that involves the contractile strain and concentration of OH^- according to Equation S5.

$$\varepsilon(c) = \varepsilon_{\text{max}} \left(1 + \frac{K}{c} \right)^{-1} \quad (\text{S5})$$

In this equation, K is the concentration of the OH^- ions at mid-strain. Specifically, it can be expressed as $K \equiv 10^{\text{pH}_{\text{mid}} - 14} = 2.5 \times 10^{-5} \text{ M}$.

144 **Modeling the bending of the asymmetric pH-responsive hydrogel.** Experimentally,
145 basic solutions at pH 12 were injected at a flowrate of either 0.15 mL/min (or the
146 equivalent of 0.3 $\mu\text{M/s}$ of OH^- ions) or 0.25 mL/min (or the equivalent of 0.5 $\mu\text{M/s}$ of
147 OH^- ions). Assuming good mixing of the medium, we used this increase in concentration
148 of the OH^- ions as the boundary condition of the surface of the hydrogel that is exposed to
149 the surrounding medium. The surface coated with the elastomer has an impermeable
150 boundary condition. The model only has one fitting parameter: the diffusion coefficient D
151 $= 5 \times 10^{-11}$ m^2/s . The order of magnitude of this diffusion coefficient agrees with that of
152 small molecules diffusing in a hydrogel (49). For the numerical solution, we assumed a 1-
153 dimensional model because the length of the hydrogel is far larger than its thickness. With
154 this slender body approximation, the dominant strains occur along the lengths of the gel
155 strip and transverse contraction is negligible in comparison. Furthermore, the strains occur
156 in regions where the ligands have already been reacted; therefore, they do not affect the
157 advancing reaction front or the diffusive characteristics of the analyte.

158 The concentrations c and s with respect to x and t were obtained by solving numerically
159 the system of Equations (1) and (2) stated in the main text. After solving these equations,
160 we used the solution of the concentration, c , for calculating the curvature of the hydrogel,
161 κ , with t via Equation 3 for both the two rates of injection. The results obtained from
162 modeling the bending of the asymmetric pH-responsive hydrogel agrees well with the
163 experiment data (Fig. 4B-C of the main text). This agreement supports the hypothesis that
164 the fundamental mechanism for the bending of the hydrogel results from the asymmetric
165 unsteady-state reaction diffusion of OH^- ions into the pH-responsive hydrogel. On the
166 other hand, we observe the general loss of curvature toward the ends of the length of the
167 hydrogel especially during high degrees of curling at later times. This deviation can be
168 attributed to several possible reasons, such as the tendency to have a more uniform

169 concentration at the ends of the hydrogel due to the diffusion at the edges (i.e., the
170 assumption of 1-dimensional diffusion is not valid at the edges) and structural non-
171 homogeneity of the hydrogel. In addition, the model did not take into account the transport
172 limitations when the hydrogel bends and rolls over itself with the impermeable coating of
173 elastomer facing outward; this form of transport limitation increases the time needed for
174 the hydrogel to straighten back out.

175 Some previous studies have reported and modeled materials that swell, bend, and
176 subsequently flatten (e.g., the wetting of paper by water) (50, 51). These studies, however,
177 involved only the absorption of the whole liquid medium (i.e., as opposed to the diffusion
178 of only one solute species in the liquid medium in our study) into the matrix of the
179 material. Hence, these previous studies did not consider any differences in the external
180 conditions at all (e.g., including any difference in the rate of bending with a difference in
181 stimulus).

182 **3. Theoretical Analysis of the Process**

184 **Detailed analysis of the reaction-diffusion process.** We analyzed the reaction-diffusion
185 process of the analyte into the asymmetric stimuli-responsive hydrogel. As the analyte
186 (e.g., OH⁻ ions) diffuses into the stimuli-responsive hydrogel, the analyte reacts with the
187 stimuli-responsive functional groups of the hydrogel, thus allowing the hydrogel to
188 contract. The reaction involved within the stimuli-responsive hydrogel is typically very
189 fast; hence, the process is usually diffusion limited. This diffusion-limited transport of the
190 analyte establishes a distinct reaction front: the unreacted functional groups at a localized
191 region within the hydrogel needs to be fully reacted before the analyte can diffuse farther
192 into the depth of the hydrogel for interacting with the unreacted functional groups.

193 Therefore, the region from the surface of the hydrogel to the reaction front (i.e., the

penetration depth, δ) consists of reacted groups, whereas the region beyond the reaction front consists of unreacted groups. The rate at which the number of moles of the stimuli-responsive functional groups are reacted per unit area (i.e., the “molar flux”, $N_{reaction}$) is related to the velocity of the penetration depth moving into the bulk of the hydrogel, $d\delta/dt$ and the molar density of the unreacted groups, s_0 , initially in the hydrogel according to Equation S6.

$$N_{reaction} \sim s_0 (d\delta / dt) \quad (S6)$$

On the other hand, the molar flux of the diffusing analyte, N_a , is defined according to Equation S7.

$$N_a \equiv -D \frac{\partial c}{\partial x} \sim -\frac{D (dc_s / dt)}{d\delta / dt} \quad (S7)$$

$\partial c / \partial x$ is the spatial concentration gradient of analyte and D is the diffusion coefficient. Applying chain rule on the spatial concentration gradient yields the relationship between the molar flux of the diffusing analyte, the penetration depth, and the rate of change of concentration at the surface of the hydrogel, dc_s/dt (i.e., the temporal concentration gradient of the analyte in the medium). Balancing the fluxes defined in Equations S6 and S7 by $N_{reaction} + N_a = 0$, we obtain the expression for the velocity of the penetration depth, $d\delta/dt$, as stated in Equation S8.

$$d\delta / dt \sim \sqrt{\frac{D}{s_0} (dc_s / dt)} \quad (S8)$$

Therefore, the velocity of the penetration depth, $d\delta/dt$, scales to the square root of the temporal gradient of concentration in the medium, dc_s/dt . We verified these scaling arguments by solving numerically the unsteady-state reaction-diffusion equations. We found that the velocity of the penetration depth does scales with the square root of the temporal gradient (Fig. 4d in the main text). Importantly, the velocity of the penetration

217 depth is closely associated with the rate of bending because the region within the
 218 penetration depth involves the reacted functional groups in the hydrogel; that is, the
 219 contracted portion of the hydrogel. Rearranging Equations S6, S7, and S8, we found that
 220 the spatial gradient of the concentration also scales with the square root of the temporal
 221 gradient of concentration according to Equation S9.

$$\frac{\partial c}{\partial x} \sim \sqrt{\left(\frac{s_0}{D}\right)}(dc_s / dt) \quad (\text{S9})$$

223 We further analyzed the curvature of bending of the hydrogel due to the reaction-
 224 diffusion process. We first note that the penetration depth, δ , that separates the regions of
 225 reacted and unreacted groups throughout the thickness of the stimuli-responsive hydrogel
 226 determines the amount of bending of the hydrogel. Assuming that the OH^- concentration is
 227 large compared to the mid-strain concentration (i.e., $c > K$), so that the contractile strain is
 228 at its maximum within the penetration zone $\varepsilon|_{(h/2-x)<\delta} \approx \varepsilon_{\max}$, negligible elsewhere
 229 $\varepsilon|_{(h/2-x)>\delta} \approx 0$, and that the active reaction zone is thin due to fast reaction, the moment of
 230 integration of concentration can be approximated according to Equation S10. h is the
 231 thickness of the hydrogel.

$$2 \int_{-h/2}^{h/2} \varepsilon x dx \approx \varepsilon_{\max} \delta (h - \delta), \quad (\text{S10})$$

233 Based on Equation S10, we can simplify the expression of the curvature, κ (i.e., Equation
 234 3 in the main text) based on the slender body approximation (in which the strains are
 235 dominant along the length relative to the transverse contraction) to Equation S11.

$$\kappa(t) \sim 6\varepsilon_{\max} h^{-3} \delta (h - \delta). \quad (\text{S11})$$

237 Equation S11 shows the relationship between the curvature of the hydrogel and the
 238 penetration depth δ . By taking the derivative of the curvature with time, we can express
 239 the rate of change of curvature according to Equation S12.

$$d\kappa / dt(t) \sim 6\varepsilon_{\max} h^{-3} (d\delta / dt)(h - 2\delta) \quad (\text{S12})$$

Equation S12 shows that the maximum curvature of the hydrogel is $\kappa_{\max} = 3\varepsilon_{\max} / 2h$, when the penetration depth is half the thickness of the hydrogel (i.e., $\delta = h/2$). If the penetration depth is small (i.e., $\delta \ll h/2$), the rate of change of curvature, $d\kappa/dt$, becomes linearly proportional to the penetration velocity, $d\delta/dt$. Under this condition, we can use the relationship between $d\delta/dt$ and dc_s/dt according to Equation S8 together with Equation S12 for obtaining the relationship between the rate of change of curvature and the temporal gradient of concentration as expressed in Equation S13.

$$d\kappa / dt \sim \sqrt{\left(\frac{36D\varepsilon_{\max}^2}{s_0 h^4}\right)} (dc_s / dt) \Big|_{\delta \ll h/2} \quad (\text{S13})$$

Equation S13 suggests that the rate of change of curvature of the hydrogel scales with the square root of the temporal concentration gradient at early times of diffusion. We verified this scaling relationship by solving the model established in the previous section numerically. This result is shown in Fig. 4f in the main text.

4. Self-regulation

As discussed in the main text, the controller can be pre-programmed to control the pH of the medium at another desired set point by modifying the system. There are potentially many parameters of the system that can be changed for varying the set point. Some of them are expected to be highly sensitive and can change the set point dramatically. For the parameters related to the asymmetric stimuli-responsive hydrogel, some examples include the type of molecular monomers used for polymerizing the hydrogel, comonomers, proportion of the different components before polymerization, type of elastomer, and thicknesses of the hydrogel and elastomer. For example, besides the pH-responsive

263 hydrogel that expands in an acidic medium, we could use a pH-responsive hydrogel that
264 expands in a basic medium instead (52). In this case, the set point of pH in the medium is
265 expected to be very different. Other types of parameters include the volume of the
266 reservoir, the concentration and type of chemicals in the reservoir, and the volume of the
267 surrounding medium. For example, if the reservoir contains a highly basic rather than
268 acidic solution, the set point is expected to change dramatically. Another example includes
269 the same system except for a much larger volume of the surrounding medium than that
270 studied in this work. In this case, the set point of the pH is expected to be more basic
271 because the small amount of concentrated acid released from the reservoir will not be able
272 to influence the surrounding medium as much as it did in the original system.

263
264
265
266
267
268
269
270
271
272
273
274
275
276

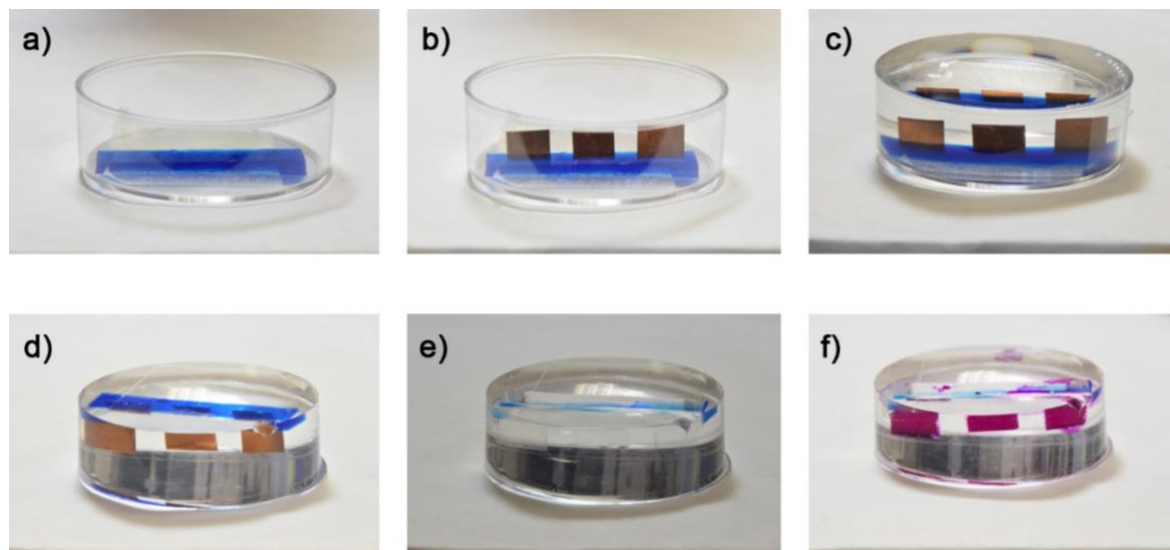


Fig. S1. Method for fabricating the PDMS molds for preparing the stimuli-

responsive hydrogels. (a) A blue-colored PDMS strip was first prepared and adhered onto the bottom of a Petri dish by double-sided tape. (b) Copper foils (5 mm x 6 mm x 100 μ m) were inserted into the blue-colored PDMS vertically. (c) Mixture of the liquid monomer and cross-linker of PDMS was degassed and filled into the Petri dish, and subsequently baked. (d) The block of polymerized PDMS was extracted out from the Petri dish. (e) The blue-colored PDMS and the copper foil were removed, leaving behind the open slits. These slits served as the molds for preparing the stimuli-responsive hydrogels. (f) As a demonstration, rhodamine B dye (red) was injected into the molds. Photo Credit: Spandhana Gonuguntla, National University of Singapore.

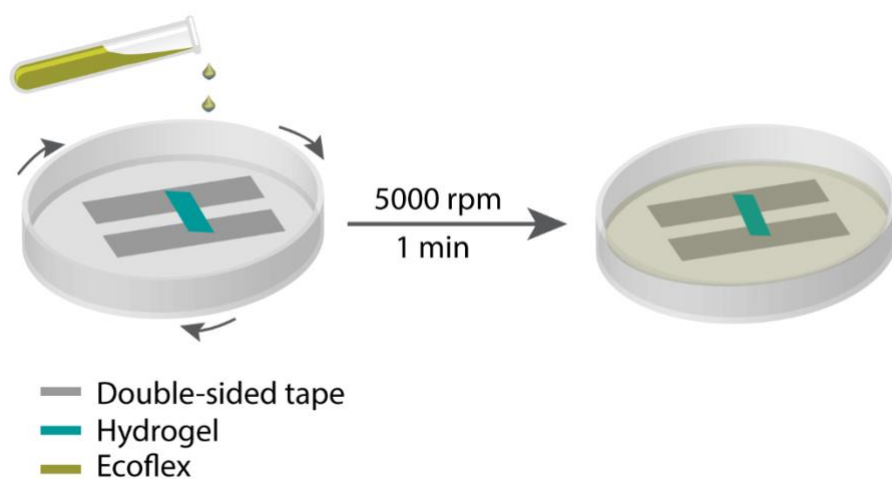
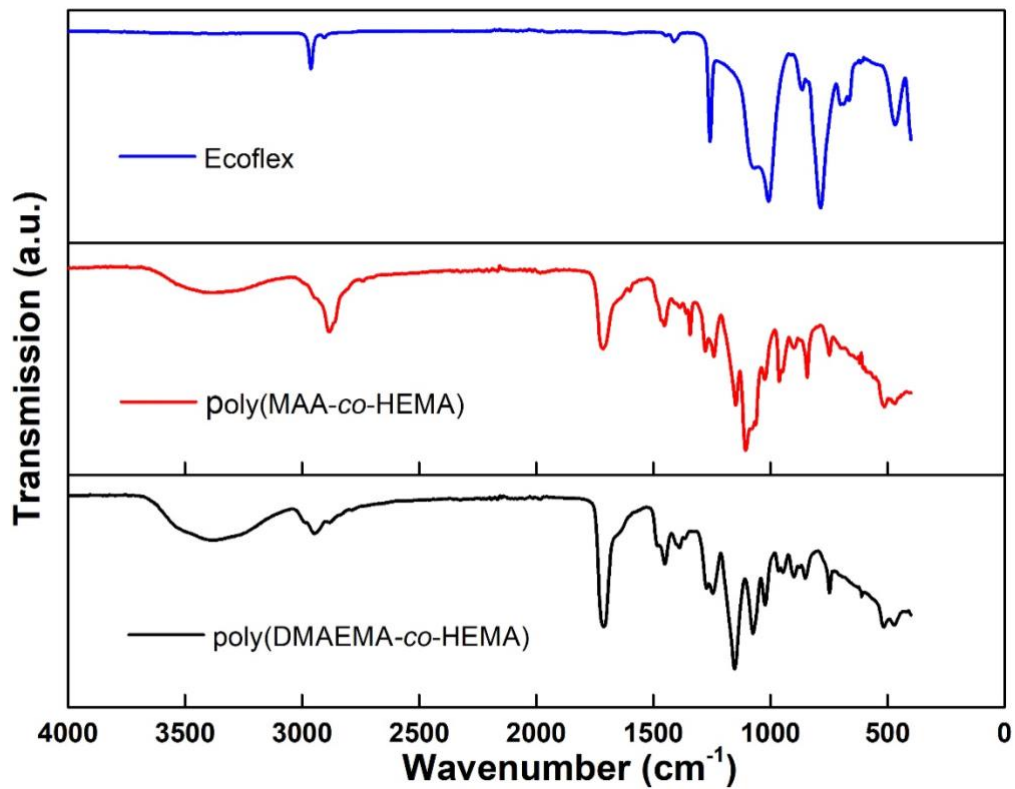
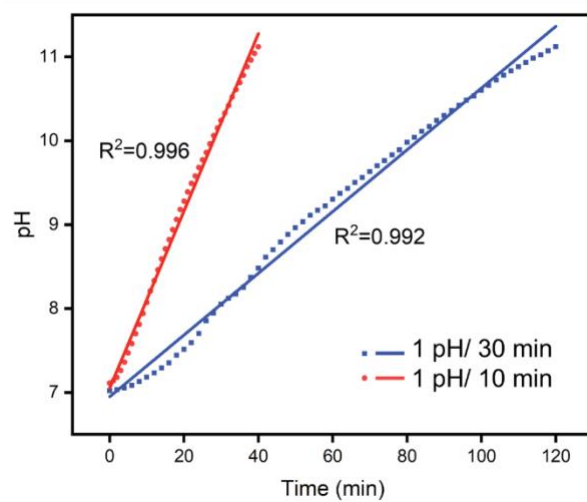


Fig. S2 Illustration showing the procedure for coating the surface of the stimuli-responsive hydrogel with a layer of elastomer. The hydrogel was first polymerized and adhered onto the bottom of a Petri dish. Liquid monomers of the elastomer were then spin-coated over the hydrogel.



300
301 **Fig. S3. FTIR spectra of the materials used for the controller.** FTIR spectra of the
302 Ecoflex silicone elastomer (top, blue line), glucose-responsive hydrogel without the
303 enzyme, poly(MAA-*co*-HEMA) (middle, red line), and the pH-responsive hydrogel,
304 poly(DMAEMA-*co*-HEMA) (bottom, black line).
305

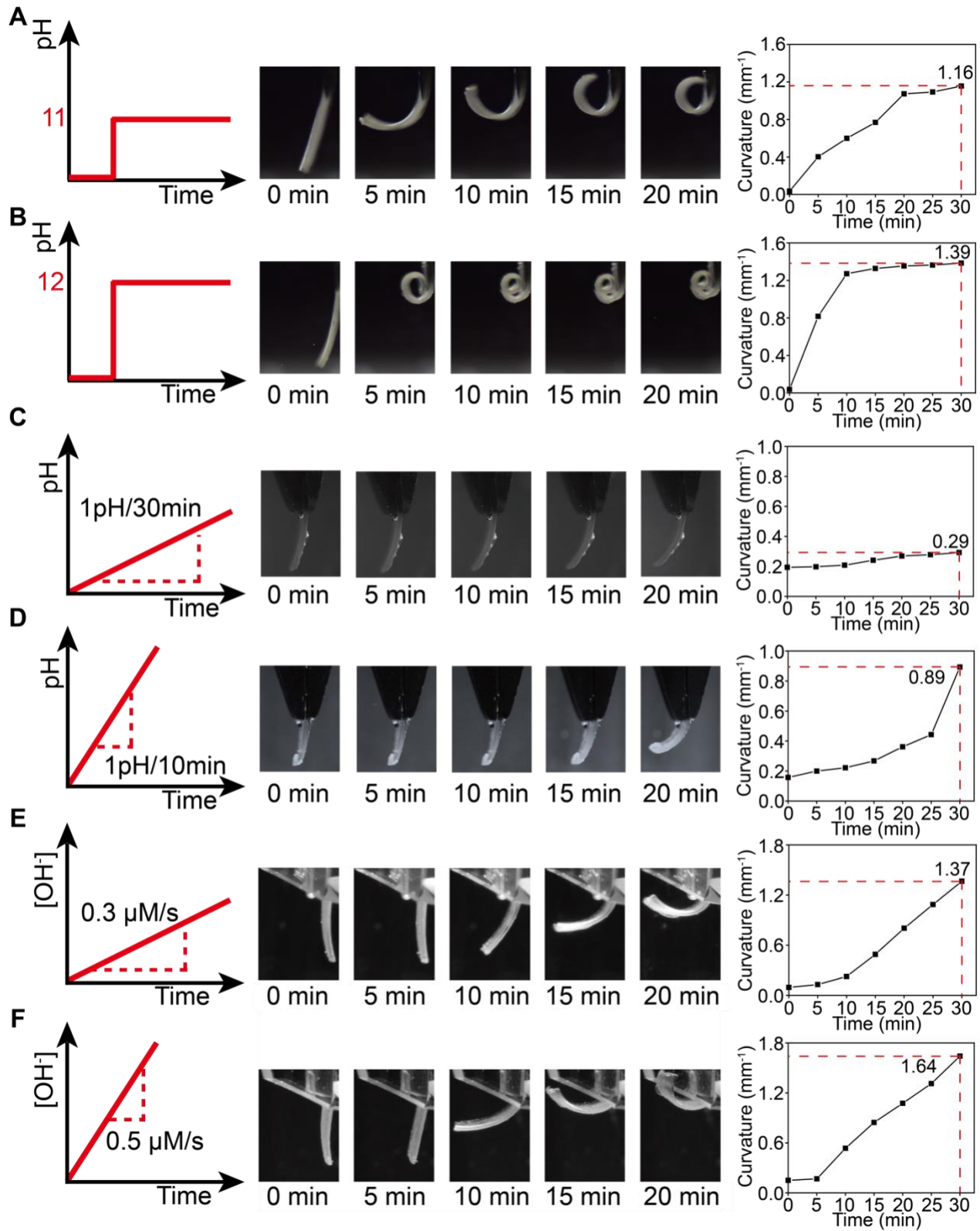


306

307

308

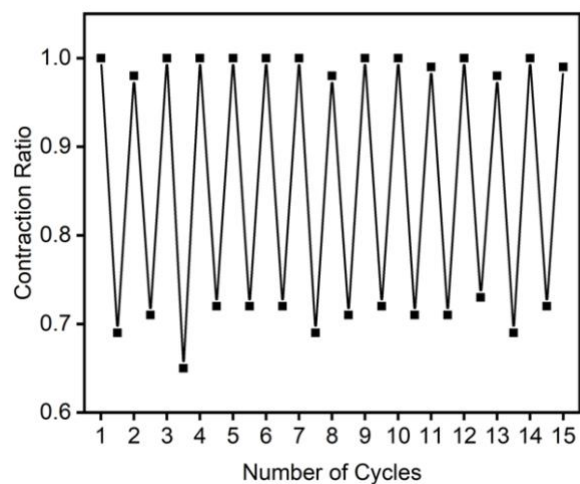
Fig. S4. Linear pH profiles with different injection rate. The R^2 values show that the pH values are fitted well with a linear trend.



309

310

311 **Fig. S5. Snapshots of the bending of the asymmetric pH-responsive materials under**
312 **different conditions with the same time points for comparison.** The asymmetric pH-
313 responsive material bent when the medium was changed (**A**) rapidly from deionized water
314 to pH 11, (**B**) rapidly from deionized water to pH 12. Bending of the asymmetric pH-
315 responsive material when the pH of the medium increased linearly with time (**C**) at a rate
316 of 1 pH unit per 30 minutes and (**D**) at a rate of 1 pH unit per 10 minutes. Bending of the
317 asymmetric pH-responsive material when the concentration of OH⁻ ions of the medium
318 increased linearly with time. The concentration was changed (**E**) gradually from deionized
319 water to pH 11 by adding a pH 12 solution at 0.15mL/min and (**F**) gradually from
320 deionized water to pH 11 by adding a pH 12 solution at 0.25mL/min. The plots on the
321 right column show the changes in curvature with time for each set of time-lapse images.



322

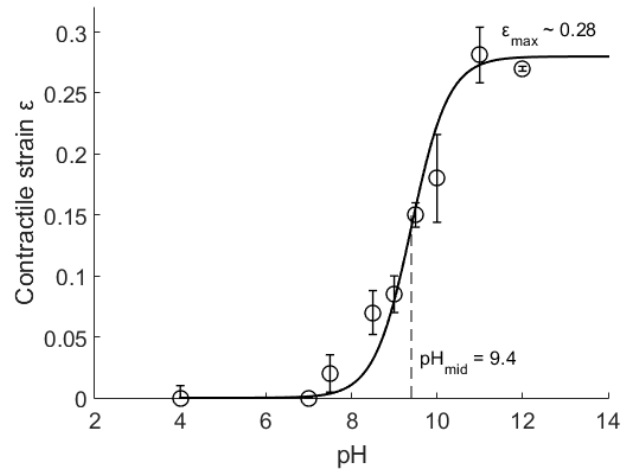
323

324

325

326

Fig. S6. Reversibility of the poly(DMAEMA-co-HEMA) hydrogel. The hydrogel could reversibly expand in an acidic solution (i.e., pH 2) and contract in a basic solution (i.e., pH 12) for at least 15 cycles.



328

329

Fig. S7. Fitting the variation of contractile strain with pH with a logistic model. The

330

circles represent the experimental data derived from the contraction ratio with different

331

pH. The solid line corresponds to the fitted logistic function.

332

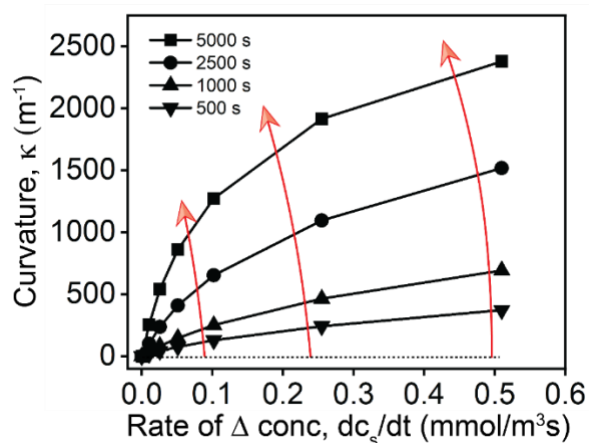
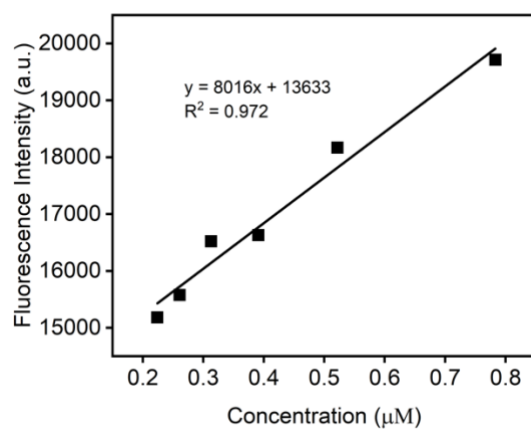


Fig. S8. Plot of the curvature against the rate of change of concentration at different times as derived from the numerical results of the model. This plot shows that the rate of change in curvature is larger when the rate of change of concentration in the medium is larger. This result is represented by the red arrows: the red arrows are longer for the same interval of time (e.g., 0 – 5000 s) when the rate of change of concentration is higher. In addition, it is also possible to deduce the rate of change of the concentration by referring to the curvature only at a specific time point by referring to this plot (i.e., under the constraints that the asymmetric stimuli-responsive material is initially flat and is still undergoing bending and not flattening).



344

345

Fig. S9. Calibration of the fluorescence intensity with the concentration of the dye.

346 **Table S1. Peak assignment table of the FTIR spectra obtained for the poly(DMAEMA-*co*-**
 347 **HEMA), poly(MAA-*co*-HEMA), and elastomer (Ecoflex™).**

Sample name	Functional groups						
	O-H	C=O	C-O	C-O-C	C-H	C-C	(CH ₃) ₂ -N
poly(DMAEMA- <i>co</i> -HEMA)	3373	1707	1154 and 1024	1075	2944	1488	1274 and 1248
poly(MAA- <i>co</i> -HEMA)	3384	1714	1022 and 1048	1106	2884	1453	x
Ecoflex™	<u>Si – (CH₃)₂</u>	<u>Si-O- Si</u>	<u>Si-CH₃</u>	<u>C-H</u>			
	784	1006 and 1070	1257	2962			

348

Table S2. Effect of different thicknesses of the layers of hydrogel and elastomer



Hydrogel thickness (μm)	Spin speed of spin coater for coating elastomer	Observation
400	5000 rpm spin speed ($< 1 \mu\text{m}$ thickness)	The asymmetric stimuli-responsive hydrogel took a few more times longer to respond and undergo a complete transition from its initial 'flat' state to the bent state, and then back to its equilibrated 'flat' state again than that reported in the main text of this manuscript.
160	5000 rpm spin speed ($< 1 \mu\text{m}$ thickness)	The asymmetric stimuli-responsive hydrogel presented in the main text of this manuscript.
160	3000 rpm	This material was not entirely <i>adaptive</i> . After the stimuli-responsive expanded in pH 12, the bilayer remained bent or exhibited deformation at the edges at steady state. 
160	1000 rpm	The layer of elastomer was significantly thicker than that used in this study. The bilayer remained bent after the stimuli-responsive expanded in pH 12 at steady state. 

Photo Credit: Spandhana Gonuguntla, National University of Singapore.